# The Post-Newtonian Three-Body Problem

Taylor Hugh Morgan

A senior thesis submitted to the faculty of
Brigham Young University
in partial fulfillment of the requirements for the degree of

Bachelor of Science

David Neilsen, Advisor

Department of Physics and Astronomy

Brigham Young University

April 2015

Copyright © 2015 Taylor Hugh Morgan

All Rights Reserved

ABSTRACT

The Post-Newtonian Three-Body Problem

Taylor Hugh Morgan
Department of Physics and Astronomy, BYU
Bachelor of Science

The gravitational three-body problem is non-analytic and exhibits chaotic behavior. Three-body interactions are common in particle-dense regions such as globular clusters and they may explain the origins of supermassive black holes. We investigate interactions in general relativity and compare them to the well understood, chaotic three-body problem in Newtonian gravity. Using the post-Newtonian equations, an approximation to general relativity, we analyzed three-body problems consisting of a binary system and a far-away, third object. We found that the system is indeed chaotic using the post-Newtonian equations. We also found that including gravitational radiation led to more black hole formations than Newtonian gravity. We also investigated possible relativistic effects on systems discovered by the Kepler Space Telescope. Particularly we looked at massive planets in tight orbits orbits and tried to refine the mass bounds of stability for the three-body systems using the post-Newtonian equations. We found that including the relativistic approximation does not significantly change the mass bounds and consumes significantly more computer resources.

Keywords: Post-Newtonian, Symplectic Integrator, Chaos, Three-Body

# ACKNOWLEDGMENTS

This material is based upon work supported by the National Science Foundation under Grant NSF PHY-1308727 to Brigham Young University. I was also funded through a BYU ORCA grant and the Department of Physics and Astronomy research assistant funding. I am very thankful for this funding. This research has been a great experience for me personally, and has opened up many doors for me.

I would like to thank my advisor Dr. Neilsen for being an amazing mentor and being so patient during the learning process. I am very grateful for the opportunity to be so involved in this research and for all of his guidance. I am so thankful for my wonderful and caring wife. She supported me during those late nights working on this research. I would also like to thank my parents for always encouraging me to follow my dreams and my sister for always challenging me intellectually.

# Contents

# List of Figures

# List of Tables

# Chapter 1

# Introduction

## 1.1 Motivation

The origin and abundance of supermassive black holes at high redshift is one of the most perplexing questions in modern cosmology. Intermediate mass black holes form due to the collision of stellar like objects such as neutron stars. Yet the lifetime of the universe, about 13.8 billion years, does not allow adequate time for enough solar-like objects to collide to form a black hole of $10^9$ solar masses in a series of binary mergers [1, 2]. In general relativity gravitational wave emission, which allows objects to dissipate energy, leads to mergers. But even this is a slow process, typically taking on the order of $10^8$ years for the merger of of an isolated neutron star binary system. However, three-body gravitational interactions provide a new mechanism for black hole formations on a much shorter time scale.

We attempt to explain the origins of supermassive black holes through numerical modeling. We created a code that solves the post-Newtonian equations, a Hamiltonian approximation in general relativity [3] for the gravitational three-body problem. Given that three-body interactions lead to more collisions between objects and gravitational wave emission also promotes collisions [4],

we have tested the hypothesis that combining the two will increase the chances of a black hole formation.

One difficulty that we face is that the three-body problem is chaotic and has no analytic solution as was shown by Poincaré in 1887 [5]. Thus we must utilize high performance computing to get an accurate picture of what effect general relativity has on the three-body problem. We have observed the chaotic nature of these systems and commented on their possible implication of supermassive black hole formation.

Using the post-Newtonian equations of motion in combination with a symplectic integrator, we have extended the scope of our research to simulate systems discovered by the Kepler Space Telescope. After the Kepler Space Telescope gathers data from observed stars it extrapolates the radius and periods of planets from the frequency and width of light curves [6]. The bounds on the mass of these planets have been calculated by using an analytic approximation to the upper mass bound [7], systematically guessing the mass of the planet around that bound, running $10^9$ orbit-long simulations, and checking for stability. They then create a range of possible masses for these planets in which the system is stable. Using the post-Newtonian equations combined with symplectic integrator we investigate whether the mass bounds of stability can be further refined for these planetary objects.

Computational difficulties have arisen with this project such as: balancing computer time with accuracy and minimizing numerical error buildup. For increased precision we typically have had to sacrifice computer time. We discuss some algorithms we have used to side-step some time-consuming numeric solvers such as compensated summation [8]. We also comment on how tests of our code using planets in our solar system.

## 1.2 The Gravitational Three-Body Problem

The gravitational three-body problem has been an important area of research since the earliest days of physics. Knowledge of the interaction of three bodies was necessary to more fully understand the Earth-Moon-Sun system. Newton treated this problem in his book *Principia Mathematica* [9], but was unable to find a solution.

The three-body problem attempts to find the future time evolution of three bodies interacting through their gravitational attraction given the initial positions and velocities of three objects. Scientists and mathematicians tried unsuccessfully to solve this problem until finally, in 1887, Poincaré proved that there is no general analytic solution in terms of algebraic operations and integrals [5, 9].

The Newtonian three-body system is now known to be chaotic [10]; an arbitrarily small change in the initial conditions can cause an arbitrarily large difference in the final outcome. The chaos in this problem has been studied abundantly [11], but little research has been done on the chaos of the three-body system in post-Newtonian gravity.

While studying the chaotic nature of the three-body problem we limit our experiments to single-star-binary interactions in which two stars are initially in a circular binary orbit, and a third star approaches from a large distance and interacts with the binary. In each experiment, one of four interactions can occur: flyby, exchange, collision, disruption, or quasi-periodic orbits. A flyby occurs when the third object flies past the binary without disrupting it, although it may change direction or become perturb. An exchange occurs when one of the objects in the binary is kicked out and the third object takes its place in the binary. Collisions between objects, or black hole formations, occur when two or more objects come within each others Schwarzschild radius. Disruption is when all three objects escape each other and fly off towards infinity. Disruptions never occur in our simulations because we have chosen the initial conditions so that the total energy of the system is less than zero.

## 1.3 Schäfer: The Post-Newtonian Equations

The scope of this thesis includes both understanding the chaotic nature of the three body problem in general relativity as well as refining the mass bounds of stability for Kepler Space Telescope systems. These two projects differ in setup and numerical methods. They do though both rely on the same fundamental set of equations. We relied heavily on work formerly done by Schäfer on the post-Newtonian equations [3, 12]. The post-Newtonian equations are a perturbation expansion of general relativity's equations of motion for a three body system. They drastically simplify the mathematical complexity of the general relativity (GR) field equations while remaining sufficiently accurate for our purposes. They rely on the assumptions that the Newtonain gravitational potential is weak ($GM/r \ll 1$, where $M$ is the total mass, $G$ is the gravitational constant, and $r$ is the separation between objects) and that the velocity, $v$, of the objects must be much less than the speed of light, $c$, ($(v/c)^2 \ll 1$). These assumptions are valid for Kepler planetary systems. For scattering experiments they may only be violated briefly during very close interactions or mergers. In the Kepler case the bodies move slow relative to the speed of light.

We use the post-Newtonian equations in the Hamiltonian $3+1$AMD formalism [3, 12, 13]. The Hamiltonian is written as a perturbation expansion in powers of $(1/c)^2$

$$H = H_N + c^{-2}H_{1PN} + c^{-4}H_{2PN} + c^{-5}H_{2.5PN}, \tag{1.1}$$

where $H_N$ is the Newtonian Hamiltonian and the others $H_{1PN}$, $H_{2PN}$, and $H_{2.5PN}$ are the approximations to general relativity at different post-Newtonian orders. Hamilton's equations give us the equations of motion, which are then integrated numerically. One way of thinking about the post-Newtonian Equations is that they are a perturbation expansion of the full set of equations in general relativity in powers of $(v/c)^2$. The factor of $(1/c)^{2n}$ for each successive term of the expansion shows that their influence is negligible in most cases, much like the higher terms in a Taylor series expansion are negligible for most applications. The reader might have noticed that

the PN2.5 order breaks the trend of the integer increase of each expansion term. This is a special term of order $(v/c)^5$ that allows for the dissipation of energy due to gravitational wave emission.

Setting up the Hamiltonian and deriving equations for their position and momentum took a significant amount of time because of the length of the equations. We solved for these in detail in Appendix A.

## 1.4 Previous Work: Setup and Initial Data

Much of this research was done in conjunction with Jared Jay [14]. His research focused specifically on expanding Boyd-McMillian's work in a 2D coordinate system. My research focuses on interaction in 3 dimensions. For both of our projects we looked at bound systems (using the same initial velocity), the same initial separation, and analyzed chaos in a similar way as Boyd-McMillian. The initial velocity was chosen such that the total energy is negative; and the derivation of this velocity is given in their paper [11]. Jay reproduces their low-resolution chaos picture in higher resolution, explores non-equal mass binaries, and the outcome of long-term runs. His paper may give some deeper insight into the mathematical nuances of the post-Newtonian equations and enunciate on the chaotic three-body problem.

My research reflects the work done by Samsing [4], who looks at 3D configurations. In my work I varied $\rho$ and $\phi$ parameters out of the plane of the binary. I also varied the percentage of the critical velocity of the third object and analyzed how this affected the chaos of the system.

# Chapter 2

# The Chaotic Three-Body Problem

In this chapter we develop the post-Newtonian equations of motion and apply them to the chaotic three-body problem. We demonstrate how to create a circular binary in the center of momentum frame using Newtonian gravity in a manner that generalizes to the post-Newtonian equations. After obtaining a relationship between radius and momentum we set up our initial conditions by adding in our third object and orienting the binary. We vary two parameters in the initial data for the third object, map out the results of each interaction, and comment on the system's chaotic nature.

## 2.1 Solving The Post-Newtonian Equations

The initial data for the chaotic scattering runs consist of a circular binary and a third object at infinity. We derive the equations of motion using a post-Newtonian Hamiltonian for a three-body system. We use a Hamiltonian formulation of the post-Newtonian equations because numerical methods that conserve the Hamiltonian are available for these systems. This will be particularly useful for the Kepler project where we run the simulations for $10^9$ orbits (Fig 3.2).

To set the initial data for the binary, we use the Hamiltonian for two bodies. Because of the complexity of post-Newtonian Hamiltonians, we illustrate the method here for Newtonian grav-

ity alone, but the same method is used for higher orders. This allows us to determine $\vec{p}$ and $\vec{q}$ (momentum and position vectors) for the binary.

The Newtonian Hamiltonian for two bodies of mass $m_1$ and $m_2$, separated by distance $r$, is

$$H = \frac{p_1^2}{2m_1} + \frac{p_2^2}{2m_2} - \frac{Gm_1m_2}{r}. \tag{2.1}$$

We restrict ourselves to the center-of-mass frame, so $p_1 = -p_2$ and let $p = \frac{p_1}{\mu}$ and $q = \frac{r}{GM}$ where $M = m_1 + m_2$ and $\mu = m/M$. The Hamiltonian then simplifies to

$$H = \mu\frac{p^2}{2} - \frac{\mu}{q}, \tag{2.2}$$

and we define a new scaled Hamiltonian

$$\hat{H} = \frac{H}{\mu} = \frac{p^2}{2} - \frac{1}{q}. \tag{2.3}$$

Hamiltonians for two bodies of this form can be found up to order 3 (PN3) [3]. We now split the momentum into radial and angular components, $p = p_r + p_\phi$. For a circular orbit, $p_r = 0$, so we have $p = p_\phi$.

We now define an angular momentum $j = qp_\phi = qp$, and insert this into the Hamiltonian.

$$\hat{H} = \frac{j^2}{2q^2} - \frac{1}{q}. \tag{2.4}$$

Now that $\hat{H}$ is in terms of $q$, we can take the partial derivative of this Hamiltonian with respect to $q$. Remember that the values of $\dot{p}$ and $\dot{q}$ are given by

$$\dot{q}_i = \frac{\partial H}{\partial p_i}, \tag{2.5}$$

and

$$\dot{p}_i = -\frac{\partial H}{\partial q_i}. \tag{2.6}$$

Evaluating Hamilton's equation for the radial momentum, which we require to be zero, gives

$$\frac{\partial H}{\partial q} = -\frac{j^2}{q^3} + \frac{1}{q^2} = -\dot{p}_r = 0. \tag{2.7}$$

Solving for $j$ gives $j = \sqrt{q}$, which in turn tells us $p = \frac{j}{q} = \frac{1}{\sqrt{q}}$. The total momentum of the first object is given by $p_1 = \mu p$. This gives $p_\phi$ as a function of radius for a circular binary. When we set up our circular binaries using the higher order post-Newtonian equations we use a similar method. Our Hamiltonians are much longer in these cases. For example, the first order Hamiltonian for two bodies is

$$\tilde{H}_{1PN} = \frac{1}{8}(3\nu - 1)p^4 - \frac{1}{2}[(3+\nu)p^2 + \nu p_r^2]\frac{1}{q} + \frac{1}{2q^2} \tag{2.8}$$

Where $\tilde{H} = (H - mc^2)/\mu$ and $\nu = \mu/m$. Compare this to the even more complicated second order approximation

$$\begin{aligned}\tilde{H}_{2PN} = &\frac{1}{16}(1 - 5\nu + 5\nu^2)p^6 \\ &+ \frac{1}{8}[(5 - 20\nu - 3\nu^2)p^4 - 2\nu p_r^2 p^2 - 3\nu^2 p_r^4]\frac{1}{q} \\ &+ \frac{1}{2}[(5+8\nu)p^2 + 3\nu p_r^2]\frac{1}{q^2} - \frac{1}{4}(1+3\nu)\frac{1}{q^3}.\end{aligned} \tag{2.9}$$

We use Mathematica to derive Hamilton's equations and generate computer code while avoiding algebra errors.

With the binary's conditions fixed, we look next at how we vary the parameter of the third object.

## 2.2 Initial Conditions

When we set up our initial conditions we fix the position of our binary as well as its radius, phase angle, and eccentricity. In order to generate readable chaos pictures we limit our variation to two parameters initially. We vary the impact parameter $\rho$ and $\theta$ of the third object. The impact parameters is the magnitude of the separation between the center of the binary and the third object and $\theta$ is the angular separation between the vertical dashed line and the third object. Figure 2.1 shows the setup for our first set of runs where the binary is in a plane perpendicular to the plane

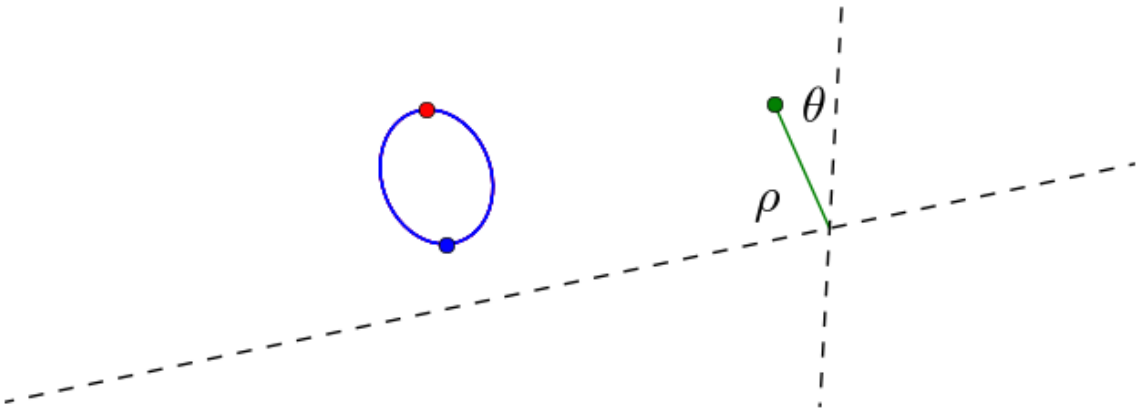


**Figure 2.1** The initial conditions for the scattering of a binary star plus a third object in 3D Cartesian coordinates.The phase angle and separation of the binary are fixed. The third object lies on a plane indicated by the dashed lines. We vary $\rho$ and $\theta$ and map out the results of each interaction based on these initial conditions. For the first set of runs the binary in the same plane as the vertical dashed line. The resulting chaos pictures are in Fig. 2.5.

in which we vary the parameters of our third object. Figure 2.2 shows a similar setup except the binary is in a plane parallel to the plane where we vary the parameters of our third object. Either way the map we generate of the results of each interaction depends on the initial position of the third object alone. I have also generated a movie, included in this thesis's .zip file, with a similar map for each slide and we vary an extra parameter, the orientation of the binary, in time.

We chose geometric units where $G = c = 1$ for these simulations as they are non-dimensional and simplify the algebra. Conversion between geometric and SI units are included in the appendix of [15]. As mentioned previously, the higher order post-Newtonian terms include factors of $c^{-2n}$ where $n$ is the order number. Thus the higher order terms quickly go to zero. We chose these units so that we can see the effects of the higher order approximations.

We positioned the third object to the right of the center of the binary at a distance of $60r$. As aforementioned, we choose the initial incoming velocity of the third object such that the total energy of the three-body system is less than zero. It can be shown [11] that this velocity must

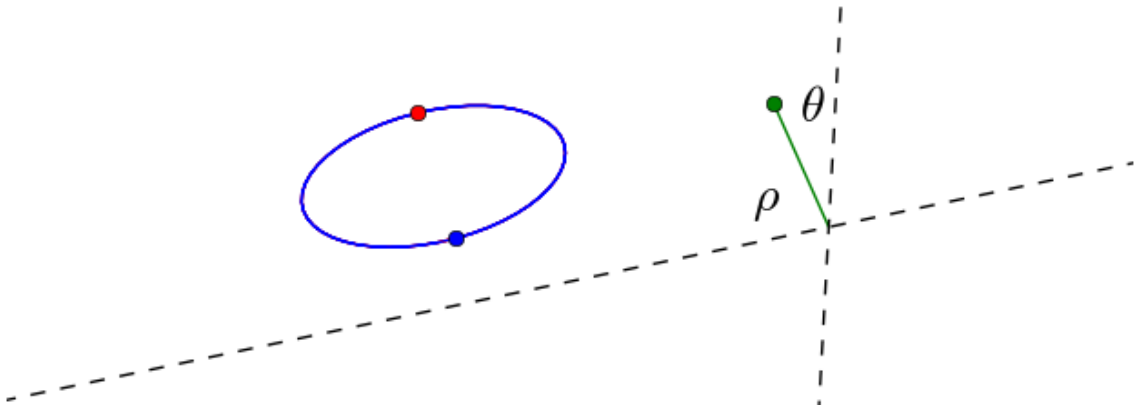


**Figure 2.2** The initial conditions for the scattering of a binary star plus a third object in 3D Cartesian coordinates for our second set of runs. They are identical to the first set of runs except the binary is now rotated 90° and is in a plane parallel to the plane where we vary the parameters of our third body. The apparent difference in size and scale of the binary's orbit is due to perspective. The resulting chaos pictures are in Fig. 2.6.

satisfy

$$v < \sqrt{\frac{Gm_1m_2(m_1+m_2+m_3)}{2rm_3(m_1+m_2)}}. \tag{2.10}$$

We set the object's velocity to one-half this value in the $-\hat{x}$ direction (approaching the binary).

## 2.3 Gravitational Radiation Terms

We include gravitational wave emission based on the work of Schäfer and collaborators, as outlined by Vilchis in his PhD dissertation [16]. These are dissipative terms that reflect the energy lost due to the gravitational waves, and are encompassed in the $H_{2.5PN}$ term of the expanded Hamiltonian. This term is unique because it first requires solving the first order approximation. Our implementation of this is found in Appendix A.

As we expect, dissipating energy from these systems acts much like frictional force. Figure 2.3 shows how a two-body circular binary loses energy as they grow closer together. Figure 2.4 demonstrates how our numerical simulation of in in-spiraling bodies matches the analytic solution. When creating our initial conditions we needed to separate the two objects in the binary such that

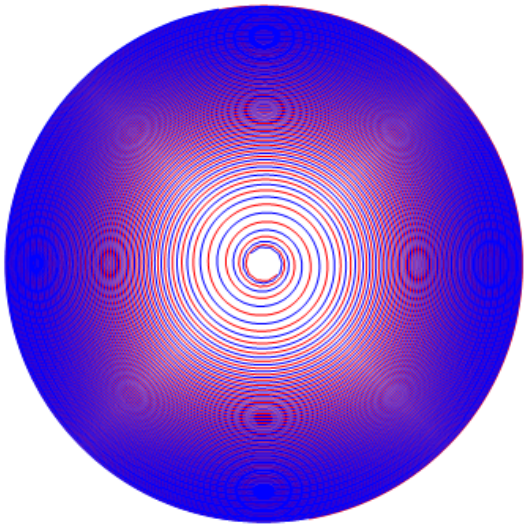

**Figure 2.3** An inward spiral of a perfectly circular binary due to gravitational radiation. The initial separation is 50 geometric units. The concentric circular wave patterns arise due to sampling frequency. They have no physical implications.

they wouldn't have the possibility to merge within the time frame of the simulation. In fact we want the in-spiraling time to be many times greater than the time frame on the simulation. The analytic solution to the orbital lifetime limits from gravitation radiation is

$$t = \frac{5}{256}\frac{c^5}{G^3}\frac{r^4}{(m_1 m_2)(m_1+m_2)}. \tag{2.11}$$

One may note that the $r^4$ term dominates especially in the case where $G = c = 1$ and $m_1 = m_2 = 1$. Thus giving $r$ the value of 100 geometric units, or about 150 km, results in an orbital lifetime of about 16 million code time units, or 77 seconds if we assume a mass scale of one solar mass. 77 seconds might not seem like much but most of the interactions happen on time scales of less than 10 s. Despite the large separation of the binary, we observe significantly more black hole formations on a shorter time scale when we include the gravitational radiation terms, as shown in Fig. 2.5 and Fig. 2.6.

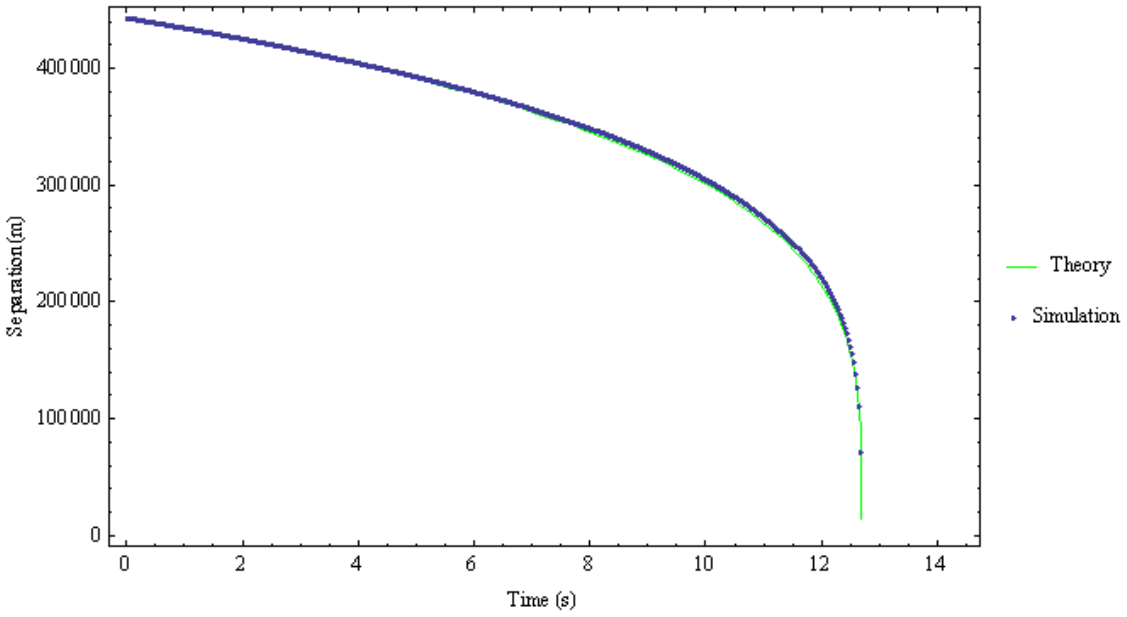


**Figure 2.4** A comparison of the numeric and analytic solution for an in-spiraling binary. We converted the non-dimensional time and length units back into SI units assuming a mass scale of one solar mass. The radius vs time matches for each case, verifying that the bodies are losing the correct amount of momentum and energy due to gravitational radiation.

## 2.4 Chaotic Scattering

Recall that our purpose is to understand the behavior of many body systems in globular clusters and to understand how general relativity might affect these systems. We believe that three-body interactions combined with relativistic effects will lead to a greater abundance of black hole formations, which is a possible explanation for the origin of supermassive black holes. We find that our assumption is correct and that there are considerably more black hole formations when we combine these two effects.

### 2.4.1 Conditions to Terminate Runs and Chaos Pictures

Now that the equations of motion are determined and the integrator is implemented, the next step is for the code to determine what was the outcome of each interaction. As mentioned previously, there are five main ways in which the binary can interact with the third star: a flyby (the third star barely perturbs the binary), an exchange (the third object switches places with one of the objects in the binary), a black hole merger (the collision of two or more objects), a disruption (which does not occur in our case because we chose the energy to be less than zero), and an in-spiral (an effect of gravitational radiation where the object lose momentum and fall inward, this occurs in the case of quasi-periodic orbits as well). We developed some algorithms in our code to determine which of these interactions occurred and so that we could exit the program promptly to save computer time. Determining collisions was fairly simple. We calculated the Schwarzschild radius, $r_{sch}$, for each object as

$$r_{sch} = \frac{Gm}{c^2}, \tag{2.12}$$

and required that the minimum separation between two stars must be the sum of their two Schwarzschild radii. If the separation became less than this amount, then a black hole formed and the code exited. This is indicated by a black pixel in the chaos images.

Flybys required the calculation of separations between each object. If one of the objects reached a distance of five times the initial separation of the binary and third object ($60r$), and had positive energy, we concluded the object had escaped. A red pixel indicates that the first object in the binary escaped, a blue pixel indicates that the second object in the binary escaped, the green pixel indicates that the third object escaped. Intuition suggests that as the third object starts farther away from the center of the binary it is more likely to escape. This is manifest in the solid green encompassing all of the images.

In the case of a flyby or exchange, we occasionally see periodic motion, where two of the objects are tightly bound and the third object orbits with a large separation. We checked for periodic motion by considering the bound system one object and the far away object as another. If the separation was significantly larger than the binary's semi-major axis and the orbit periodic, the code exited. This is indicated by a yellow pixel.

The following pictures show results from millions of interactions in our three-body systems. Figure 2.5 corresponds to the initial conditions of Fig. 2.1 and Fig. 2.6 corresponds to Fig. 2.2. Each pixel represents a different run with its position corresponding to the initial position of the third object and the color of the pixel represents the outcome.

## 2.5 Conclusions

We can qualitatively see that general relativity affects the chaotic nature of the three-body problem. For each approximation we see variation in chaotic regions and regions of consistency shifted. We can draw several conclusions from the qualitative chaos plots: the dynamics for post-Newtonian order one differ significantly than PN0 and PN2, there are fewer black hole formations for PN2 than for PN0, there are significantly more black hole formations when we factor in gravitational radiation, and the black holes that do form, form much more quickly than the equivalent two body

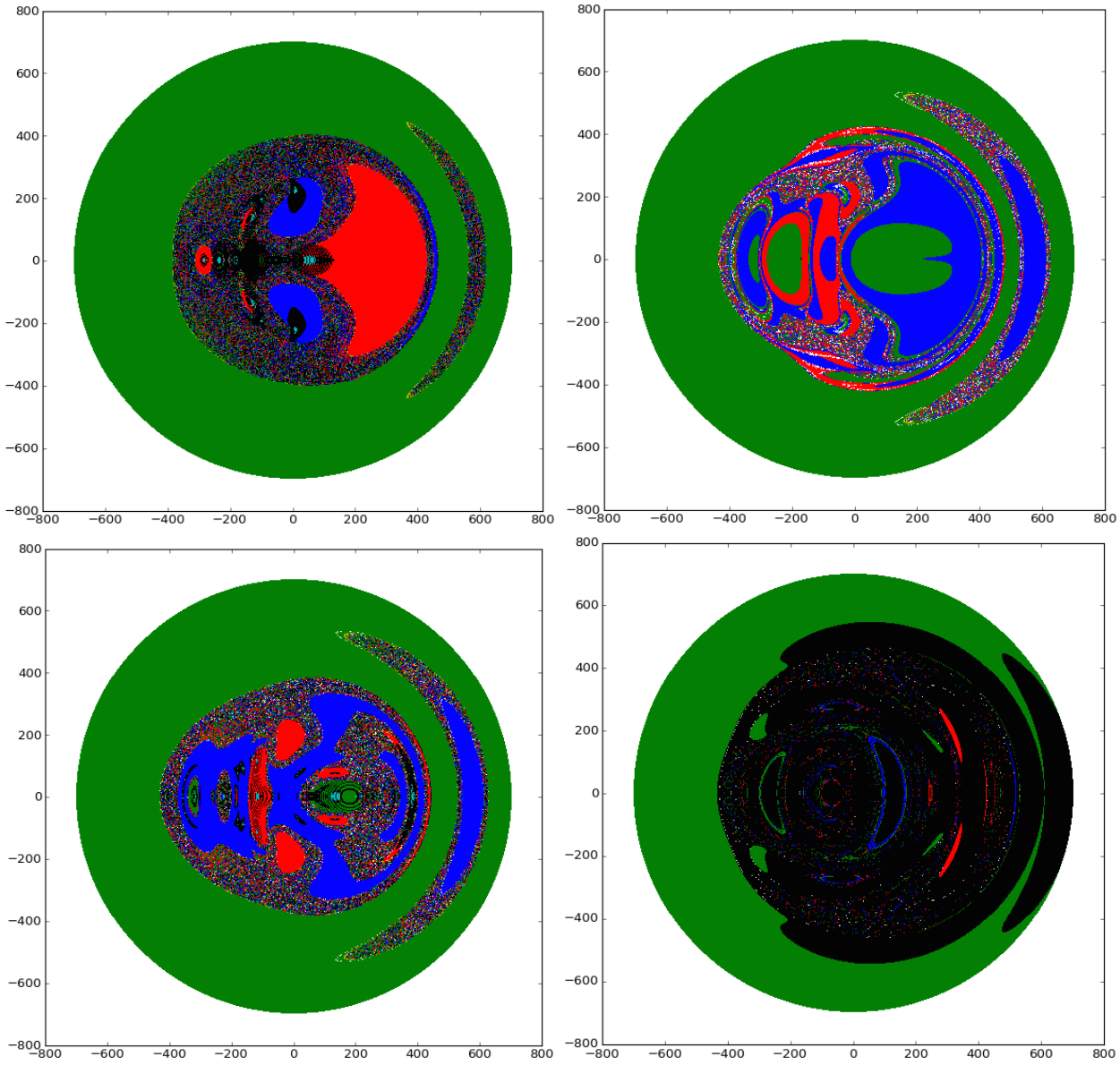


**Figure 2.5** The results of each scattering interaction for 0th, 1st, 2nd, and 2.5th order equations respectively. The initial conditions for each of these runs correspond to Fig. 2.1. The units on the axis are non-dimensional geometric units where $G = c = 1$. Notice the abundance of black hole formations for the 2.5th order equations that include gravitational radiation. Also note that the symmetry about the $x$ axis in these plots arise from the orientation of the binary in the initial conditions.

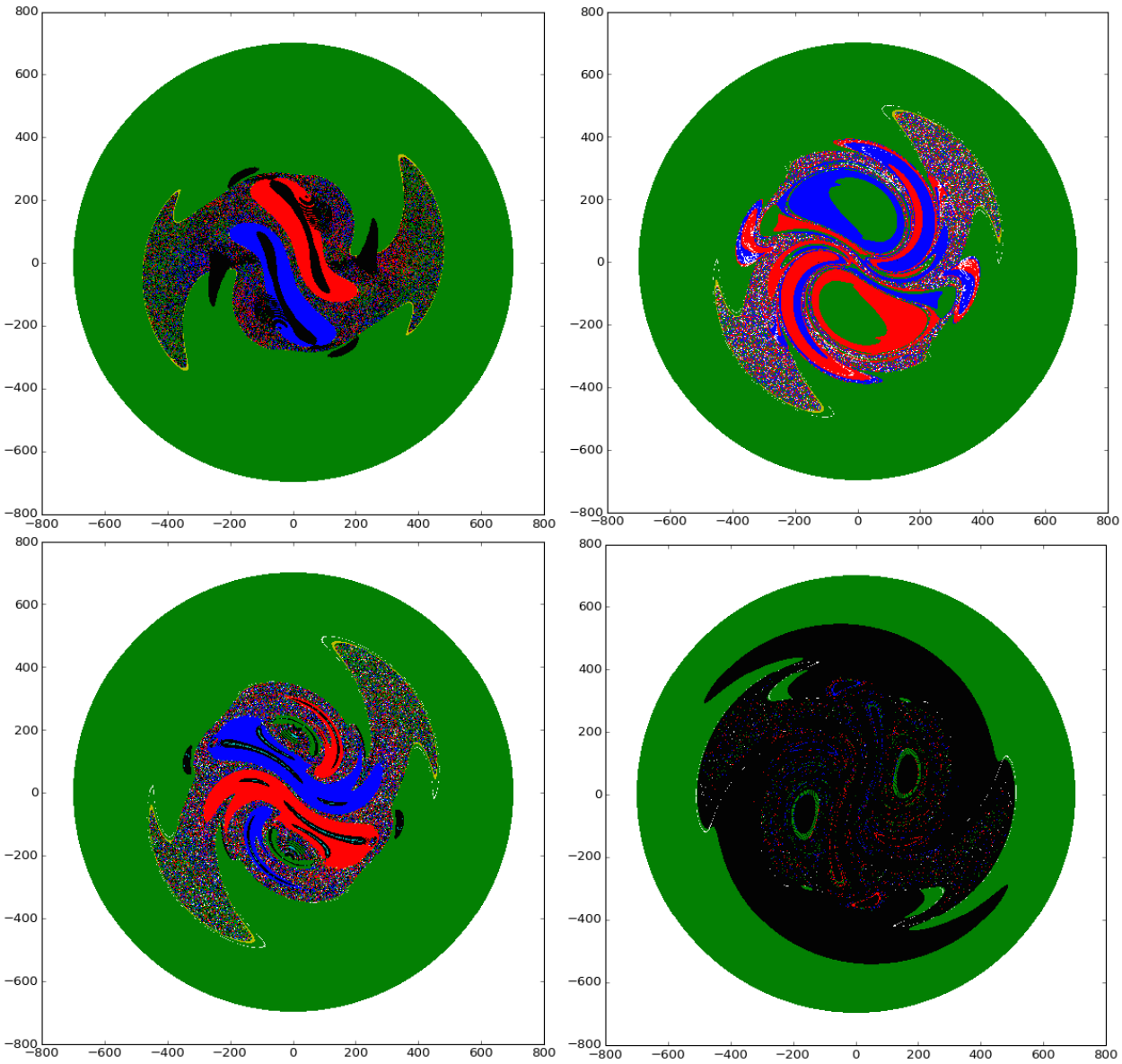


**Figure 2.6** The results of each scattering interaction for 0th, 1st, 2nd, and 2.5th order equations respectively. The initial conditions for each of these runs correspond to Fig. 2.2. The units on the axis are non-dimensional geometric units where $G = c = 1$. Notice the abundance of black hole formations for the 2.5th order equations that include gravitational radiation. Note that the non-axial symmetry of each order arises from the orientation of the binary in the initial conditions. These runs have a binary in a parallel plane and thus their symmetry is non-axial.

| Simulation | Black Holes | Runs | Black Holes(%) | Formation Time(s) |
|---|---|---|---|---|
| Scattering(PN0) | 25326 | 262144 | 9.66 | 5.12 |
| Scattering(PN1) | 14 | 258799 | 5.41e-3 | 2.28 |
| Scattering(PN2) | 15766 | 260566 | 6.05 | 7.97 |
| Scattering(PN2.5) | 103479 | 261853 | 39.52 | 0.857 |
| Perpendicular(PN0) | 19875 | 262144 | 7.58 | 6.94 |
| Perpendicular(PN1) | 2 | 258997 | 7.72e-5 | 2.57 |
| Perpendicular(PN2) | 13579 | 260608 | 5.21 | 6.92 |
| Perpendicular(PN2.5) | 92050 | 261742 | 35.17 | 0.889 |

**Table 2.1** A comparison of the number of black hole formations for each setup and order. Scattering corresponds to the initial setup described in Fig. 2.1. Perpendicular corresponds to the initial setup described in Fig. 2.2.

problem with gravitational radiation.

Something that we noticed early on in the testing process is that the PN1 equations lead to different dynamics than PN0 or PN2. Before two objects get within their Schwarzschild radii, they quickly repel each other, and then shoot off. Taking a closer look at the two-body Hamiltonian shows that this is an effect of the effective potential, which goes to negative infinity as r goes to zero. Thus it appears like the Hamiltonian shoots off to positive infinity at some point before the Schwarzschild radius. This is where the objects receive all of their energy. These results from the first order approximation are non-physical as they arise when the conditions used to derive the post-Newtonian approximation ($GM/r \ll 1$ and $(v/c)^2 \ll 1$) are not met. Thus we ignore the physical implications of this approximation. The chaotic nature of this set of equations is nonetheless interesting.

The number of black hole formations is shown in Table 2.1. The number of black hole formations is roughly equivalent for PN0 and PN2. There are, though, slightly fewer black hole

formations for PN2 than Newtonian gravity. A possible explanation, which we explore more in chapter 3, is that general relativity stabilizes three-body systems. More work needs to be done in this area.

As the reader can see from Table 2.1, there are significantly more black hole formations when gravitational wave emission is included. A skeptic may argue that the black hole formations are due to the bodies spiraling inward because of allotted time. For the two-body problem the inspiral time is 77 seconds. The time in which the formations occur is less than one second for PN2.5. Thus the the abundance of black hole formations is not due to energy loss through gravitational waves alone, but a combination of that and the three body interactions.

Thus three body eeffects can lead to black hole formations at a much shorter timescale than for the two body problem. The origins of supermassive black holes is resolved! Not quite. Before any definitive conclusions are drawn, some more work needs to be done. The next step is to factor in angular momentum of the neutron star-like objects. This will affect the trajectories and the potential energies of these objects. We need to be able to do N-body (globular cluster) simulations with gravitational radiation, which is not possible at this time. These results indicate however that gravitational wave emission and N-body interactions lead to increased supermassive black hole production.

# Chapter 3

# Kepler Systems: Refining Mass Bounds

The Kepler Space Telescope mission has searched for exoplanets, or planets orbiting around other stars. It has, to date, discovered 4178 planetary candidates, 2165 eclipsing binary stars, and confirmed 1019 planets [17]. Its mission is to search for earth-like planets and understand how solar systems evolve. A crucial part of this mission is determining the mass of the discovered planets. Previous work has involved finding the mass upper bound for a stable system using Hill stability [7]. To verify the analytically derived upper mass bound, these systems were evolved using Newtonian gravity over $10^9$ orbital periods and checking to see if the system is stable [6].

We investigate three-body systems discovered by the Kepler Space Telescope and whether including higher order relativistic terms modifies the mass bounds. The assumption was that relativity would stabilize higher mass systems. This is due to the fact that resonances are modified in general relativistic systems due to orbital precession. We have determined that the mass bounds cannot be further refined using the post-Newtonian equations because the effects of general relativity are minimal even for solar-like stars with Jupiter-mass planets within Mercury's radius.

## 3.1 The Kepler Space Telescope

The data for our modeled systems are taken from the Kepler Space Telescope mission. The telescope looks at a region of space for days at a time over which it gathers light from nearby stars. As planets pass between the star there is a noticeable dip in the light intensity received the star. Figure 3.1 illustrates the way data acquired by the telescope is analyzed to detect planets. Given that dip in the light curve, astronomers can deduce several properties of the transiting planet: radius, orbital period, orbital inclination, semi major axis, etc.

For our work we took orbital period, radius of the planet, and orbital inclination from the NASA Kepler database [17] to generate our initial conditions. Previously Kepler planet simulations have been initialized using two-body Kepler laws in order to determine semi-major axis from period. We use the post-Newtonian two-body equations to determine semi-major axis from period assuming a circular orbit.

## 3.2 The Symplectic Integrator

Numerical solutions of periodic systems for extremely long times are difficult to obtain. Numerical errors usually grow as $O(t^p)$ which can significantly corrupt the solution. The LSODA [18] integrator was used for the chaos project described in Chapter 2. The LSODA integrator uses an adaptive time step and it can be applied to both stiff and non-stiff ODEs. For our scattering runs under the chaos project, this was very useful because a third body started from far away at low velocity, had a close interaction with the binary at high velocity, and often became close enough to form a black hole. However, numerical errors in LSODA degrade the solutions of periodic systems over periods of 10 million years. To evolve Kepler systems we also need the numerical error to be minimal and need to compensate for the numerical buildup that happens over $10^9$ orbital periods.

Thus we began experimenting with different integration methods. We found the symplec-

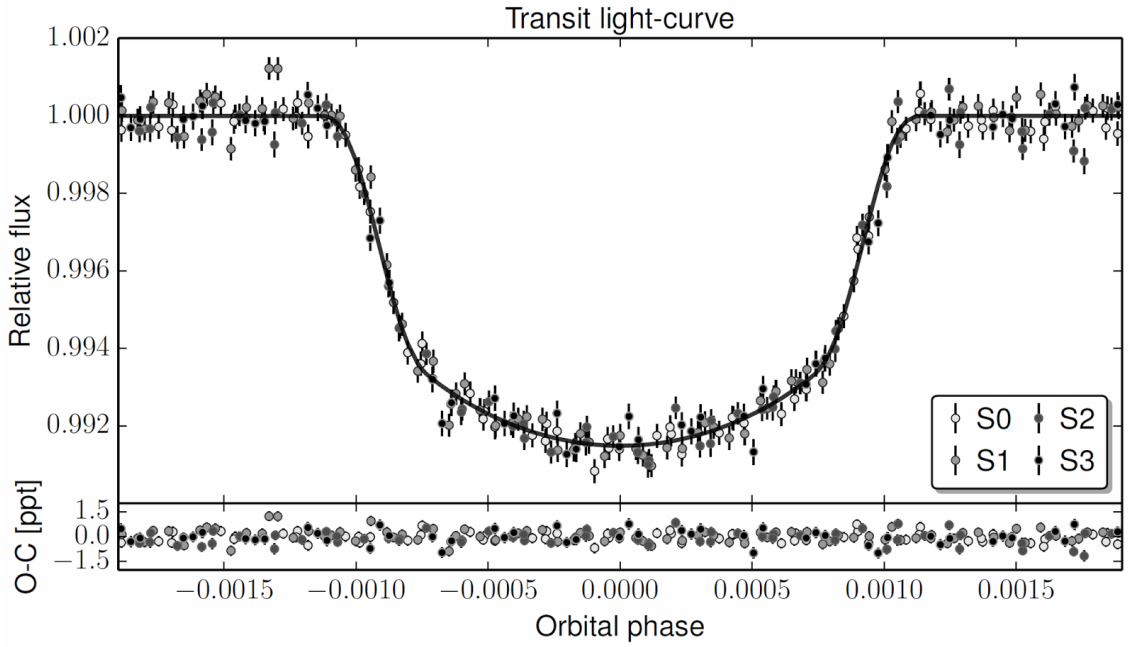


**Figure 3.1** A light curve taken by the Kepler Space Telescope database [17]. From this data the approximate radius of the planet and orbital parameters such as period, eccentricity, and inclination can be extrapolated.

tic integrator had a lot of potential as well as an integrator called ODEX [19] which utilizes the Bulirsch−Stoer algorithm. A symplectic integrator is designed to conserve the value of the Hamiltonian, which in the energy in this case. The post-Newtonian equations up to order 2 conserve energy and angular momentum. One disadvantage of the symplectic integrator is it requires a fixed time step. Moreover, given the complexity of the equations we must use an implicit integration scheme. We experimented with 4th, 8th, 12th, and 16th order Gauss-Runge-Kutta methods. We found that the solution did not significantly improve with the 16th order Gauss-Runge-Kutta method as compared to the 12th order.

To make sure that our code was producing physical results, we tested it using the orbital parameters of Mercury and Venus. When using the LSODA [18] integrator, we found that Mercury's orbit experienced a non-physical amount of precession in just over a few million years. The ODEX integrator resulted in less precession and took less time, yet we were unsatisfied with that degree

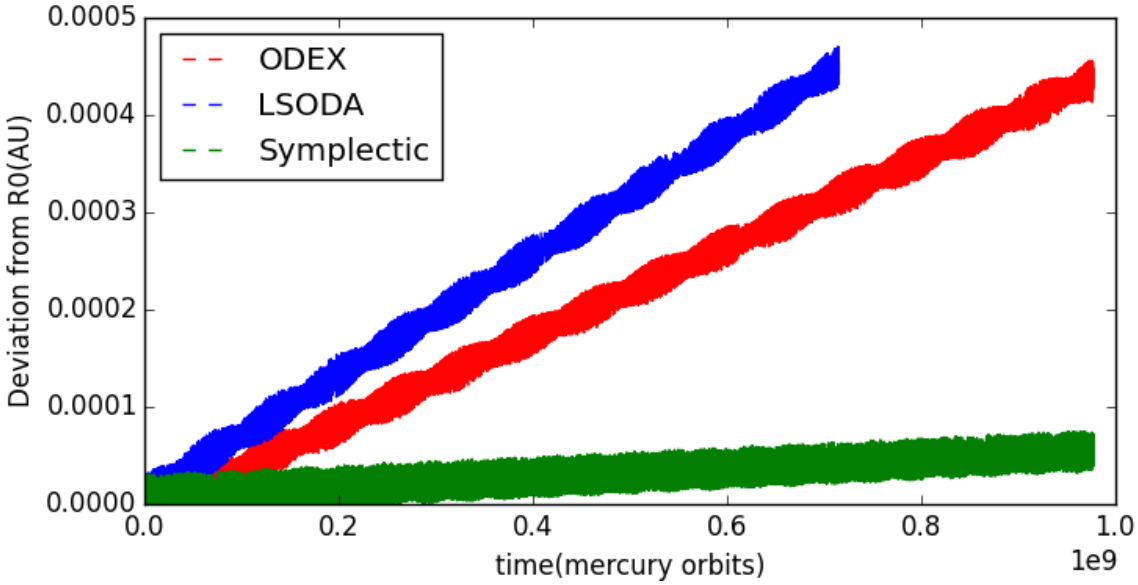


**Figure 3.2** A comparison of precession in the Mercury-Venus-Sun system using LSODA (our adaptive time step integrator) vs ODEX (the BulirschStoer method) vs the symplectic integrator in Newtonian gravity over $10^9$ mercury orbits. LSODA failed before it reached $10^9$ orbits. The orbit of Mercury precesses fastest for LSODA and ODEX due to numerical buildup. The symplectic integrator remains fairly stable. One possibility of why there is less numerical buildup for the symplectic integrator is the use of extended precision and compensated summation.

of numerical error buildup. With the symplectic integrator we found that Mercury's orbit was very stable and did in fact experience very little precession. Figure 3.2 illustrates how numerical error builds up for the three methods. To evolve the system for very long times, however, we had to use additional methods to minimize the numerical error. When we could evolve the Mercury-Venus-Sun system for over $10^9$ orbital periods we knew that the code was stable.

## 3.3 Minimizing Numerical Error

To minimize the accumulation of numerical error we used several algorithms described by Hairer [8]: compensated summation, iteration until convergence, split coefficients, and extended precision. We will comment on these methods briefly, but the reader is encouraged to explore [8] for

a deeper discussion. Iteration until convergence forced the integrator to take more steps until the error was machine zero or until the error started rising. Split coefficients represents coefficients as an exact finite precision number plus a small correction. It was built with the intention to run on a Xeon phi co-processor, and we did find that there was about a 20% speedup on these chips. We cannot use it though for more than one job at a time because we are limited by Marylou's single Xeon phi chip. Compensated summation accumulates round-off error in a register so that, over long times, it partially cancels out. Extended precision relies on Intel x86 processors performing calculations using 80 bits of precision instead of the typical 64 bits of a double. It is very useful for this project because it does not increase the run time. The 80 bits of calculation are then saved by declaring a variable as a "long double" in C. We also experimented with quadruple precision implemented in software using the GNU Quad-Precision Library. However, this made the code run 100–1000 times slower, and thus was not of use.

## 3.4 Refining Mass Bounds

As mentioned before, the purpose of this research is to get a more accurate understanding of what masses for these planetary systems are allowed for stability. Because the three-body problem has no analytic solution, we cannot predict what will happen, and we must evolve these systems numerically. We follow the standard practice [6] and evolve the systems for $10^9$ orbits of the inner planet to determine stability. We assume that the system has gone unstable if one of the planets escapes, moves to an orbit five times its initial radius, or collides with another planet. Otherwise the system is stable for the given masses.

### 3.4.1 Hill Stability

Because the range of possible masses we can test is infinite, we would like to start with an analytical approximation and work from there. Previous work has verified [7] an analytic approximation to the mass upper bound of stability, given by the equation

$$\Delta > 2.4(\mu_1 + \mu_2)^{1/3}, \tag{3.1}$$

where $\mu_1$ and $\mu_2$ are the mass ratios of the two objects to the sun, $\Delta$ is the non-dimensional separation between the two planets assuming that the separation between the first body and the sun is 1, and 2.4 arises from the phase of the objects being 180° offset. We know $\Delta$ from Kepler data, so we rearrange the terms to give

$$\mu_1 + \mu_2 < (\frac{\Delta}{2.4})^3. \tag{3.2}$$

From this the theoretical upper limits for the mass bounds are calculated. The upper limits of the mass for Kepler 48 and 56 are given in Table 3.1.

### 3.4.2 Numerical Analysis

Because the effects of general relativity increase with higher density systems, or systems with smaller separation between objects, we examine systems with Jupiter-like planets at orbital radii less than that of Mercury. Many exoplanets discovered by the Kepler Telescope fall into this category. For the purposes of this paper we will explore relativistic effects in Kepler 48 and Kepler 56. These two systems have massive planets close to their host star. The details of these two systems are given in Table 3.1. For up-to-date information on these systems see http://kepler.nasa.gov/Mission/discoveries/.

Using this information, we create initial conditions for a three-body system and simulate it for $10^9$ orbital periods of the innermost planet [6]. Once again, the end product of this research is to determine a range of masses for which the system is stable. When running these simulations with

| Planetary Candidate | Star Mass ($M_{sun}$) | Radius ($R_{earth}$) | Period (days) | Inclination (deg) | Mass upper limit ($M_{earth}$) |
|---|---|---|---|---|---|
| Kepler 48b | 0.88 | 2.14 | 4.78 | 87.660 | 1887.83 |
| Kepler 48c | 0.88 | 3.14 | 9.67 | 89.950 | 3689.85 |
| Kepler 56b | 1.37 | 6.51 | 10.50 | 87.090 | 22.10 |
| Kepler 56c | 1.37 | 9.80 | 21.40 | 80.0210 | 181.00 |

**Table 3.1** Periods, radii, and orbital inclination are taken from NASA's Kepler Space Telescope Database [17]. We chose systems with Jupiter-mass planets within Mercury-size orbits.

Newtonian gravity, the simulation takes about one week. When running these simulations with the post-Newtonian approximations our simulations can take up to ten times longer. Because our time is severely constrained, we were limited to only testing Newtonian gravity and PN2 for Kepler 48 and 56. Figure 3.3 and Fig. 3.4 show the stability plots for Kepler 48 and Kepler 56 respectively.

## 3.5 Conclusions

For the Kepler 48 simulation, which were both successfully evolved out to $10^9$ years, it is not apparent that the post-Newtonian equations have affected the stability of masses. There are only four points out of 100 that are stable for PN2 that are unstable for PN0. Kepler 56 needs to continue to be evolved out to a billion years, but that will take another month at least. We continue to experiment, trying to speed up the code even further without a loss of numerical precision. There is still a lot of work that needs to be done. Our sample size is very small, only two systems, so we plan looking at Kepler 9, 11, 18, and 57 next. There are a plethora of similar, high-mass planets discovered by Kepler. We also want to factor in gravitational radiation. Gravitational wave emission allows energy to radiate away from this system. Over $10^9$ years enough energy may be

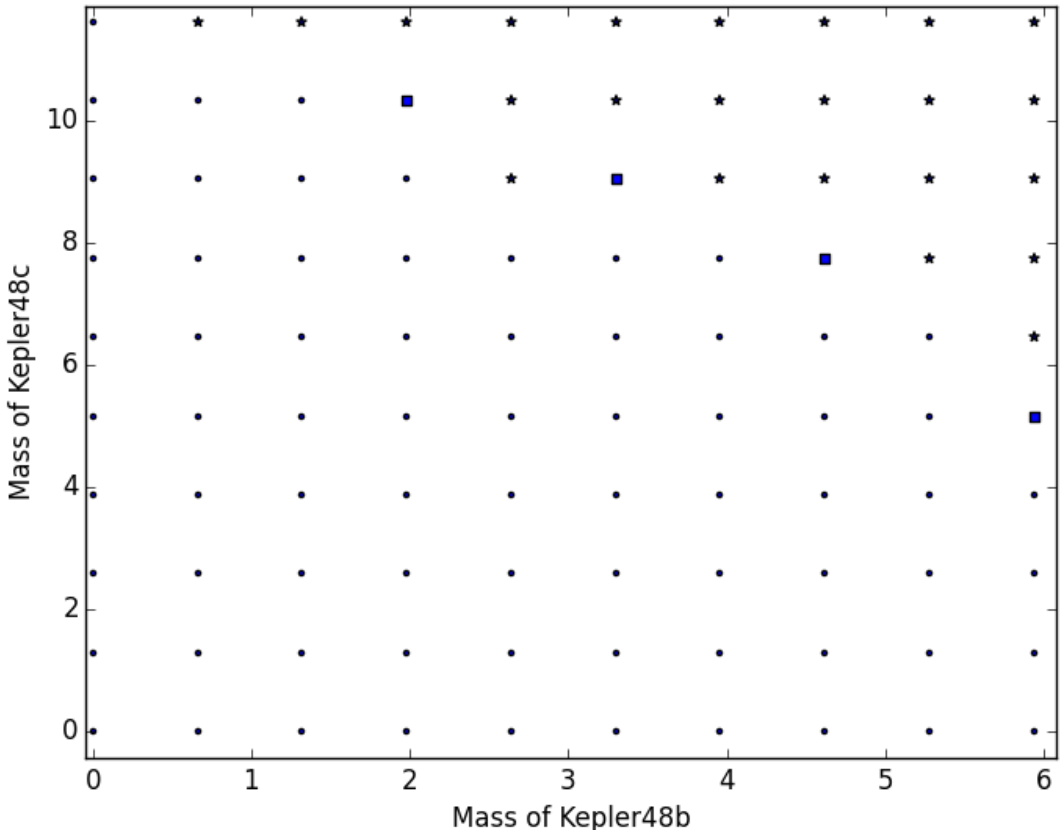


**Figure 3.3** The stability plot for Kepler 48 for Newtonian gravity and post-Newtonian order 2. We tested 100 different masses in this range. The units of the axis are in Jupiter masses. We restricted our simulation to 48b and c because they are most likely to be affected by general relativity. Stars indicate both PN0 and PN2 went unstable, blue squares indicate that PN0 went unstable but PN2 did not, blue X's indicate that PN2 went unstable but PN0 did not, black dots indicate that the run was stable for $10^9$ years. Notice that there are four points out of 100 that are unstable for PN0 yet stable for PN2. Otherwise the region of stability is the same.

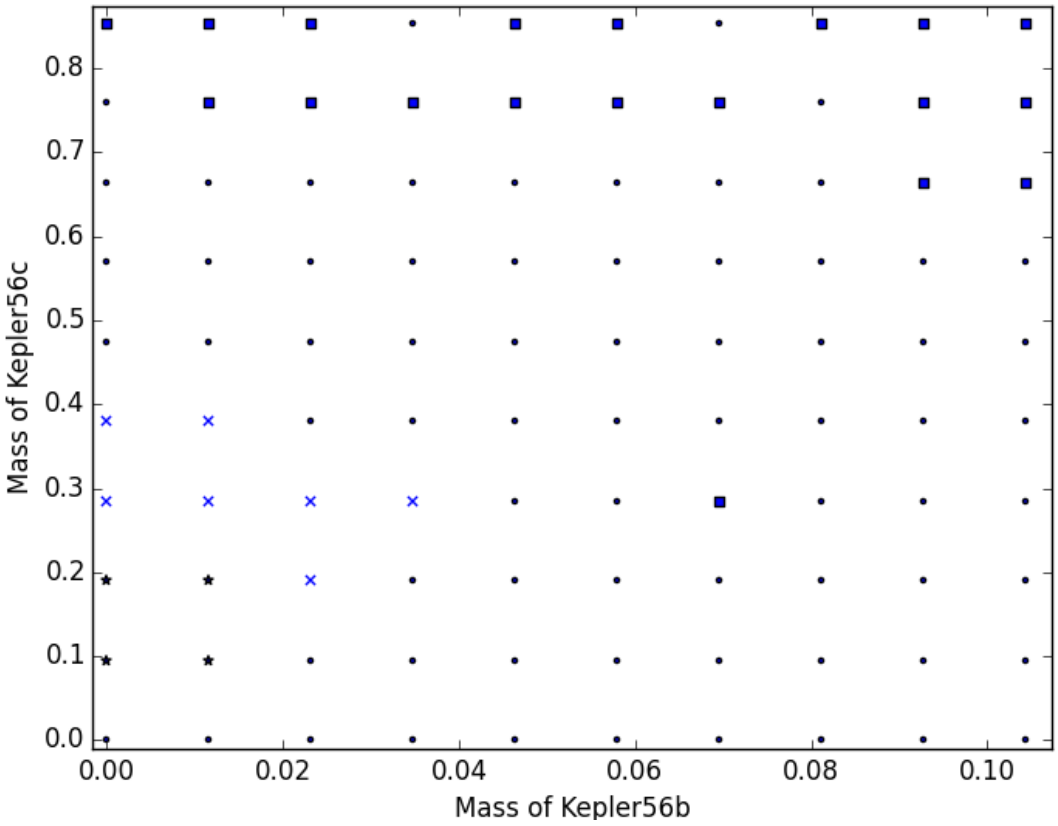


**Figure 3.4** The stability plot for Kepler 56 for Newtonian gravity and post-Newtonian order 2. We tested 100 different masses in this range. The units of the axis are in Jupiter masses. Stars indicate both PN0 and PN2 went unstable, blue squares indicate that PN0 went unstable but PN2 did not, blue X's indicate that PN2 went unstable but PN0 did not, black dots indicate that the run was stable for $10^9$ years. Note that there is a there is a region of stability for PN2 on the top that is unstable for PN0. This is because we were only able to evolve the PN2 equations out $10^8$ years. We expect that if we could evolve them out further that PN2 would go unstable there too.

radiated away that some planetary systems might settle into more stable configurations.

# Appendix A

# The Post-Newtonian Equations

This appendix give the post-Newtonian equations for three-bodies in the ADM Hamiltonaian formalism. We define $\mathbf{x}_a$ to be the three-dimensional position vector in Euclidean space for an object $a$ of mass $m_a$. We define $\mathbf{r}_{ab} = \mathbf{x}_a - \mathbf{x}_b$, $r_{ab} = |\mathbf{r}_{ab}|$, and $\mathbf{n}_{ab} = \mathbf{r}_{ab}/r_{ab}$. We define $\mathbf{p}_a$ to be the momentum of object $a$. Assuming $(v/c)^2$ is small and using a perturbation approach, the post-Newtonian system can be described by a Hamiltonian of the form

$$H = H_N + \frac{1}{c^2}H_{1PN} + \frac{1}{c^4}H_{2PN} + \frac{1}{c^5}H_{2.5PN}, \tag{A.1}$$

where $H_N$ is the Newtonian Hamiltonian and $H_{1PN}$, $H_{2PN}$, and $H_{2.5PN}$ are the approximations to general relativity to different post-Newtonian orders. The Hamiltonian equations give us the equations of motion in first-order form, which can then be integrated

$$(\dot{x}^i_a)_n = \frac{\partial H_n}{\partial p^i_a}, \tag{A.2}$$

$$(\dot{p}^i_a)_n = -\frac{\partial H_n}{\partial x^i_a}, \tag{A.3}$$

The equations of motion can be written

$$\dot{\mathbf{x}}_a = (\dot{\mathbf{x}}_a)_0 + (\dot{\mathbf{x}}_a)_1 + (\dot{\mathbf{x}}_a)_2 + (\dot{\mathbf{x}}_a)_{2.5}, \tag{A.4}$$

$$\dot{\mathbf{p}}_a = (\dot{\mathbf{p}}_a)_0 + (\dot{\mathbf{p}}_a)_1 + (\dot{\mathbf{p}}_a)_2 + (\dot{\mathbf{p}}_a)_{2.5}, \tag{A.5}$$

We now proceed to write out each order of approximation of the Hamiltonian assuming $G = c = 1$.

$$H_N = \frac{1}{2}\sum_a \frac{p_a^2}{m_a} - \frac{1}{2}\sum_{a,b\neq a} \frac{m_a m_b}{r_{ab}}. \tag{A.6}$$

The first order Hamiltonian is

$$\begin{aligned} H_{1PN} = &-\frac{1}{8}\sum_a m_a \left(\frac{p_a^2}{m_a^2}\right)^2 - \frac{1}{4}\sum_{a,b\neq a} \frac{m_a m_b}{r_{ab}} \left\{ 6\frac{p_a^2}{m_a^2} - 7\frac{\mathbf{p}_a \cdot \mathbf{p}_b}{m_a m_b} - \frac{(\mathbf{n}_{ab}\cdot\mathbf{p}_a)(\mathbf{n}_{ab}\cdot\mathbf{p}_b)}{m_a m_b} \right\} \\ &+ \frac{1}{2}\sum_{a,b\neq a,c\neq a} \frac{m_a m_b m_c}{r_{ab} r_{ac}}. \end{aligned} \tag{A.7}$$

The second order Hamiltonian is

$$
\begin{aligned}
H_{2PN} =& \frac{1}{16}\sum_a m_a\left(\frac{p_a^2}{m_a^2}\right)^3 + \frac{1}{16}\sum_{a,b\neq a}\frac{m_a m_b}{r_{ab}}\left\{10\left(\frac{p_a^2}{m_a^2}\right)^2 - 11\frac{p_a^2 p_b^2}{m_a^2 m_b^2} - 2\frac{(\mathbf{p}_a\cdot\mathbf{p}_a)^2}{m_a^2 m_b^2} + 10\frac{p_a^2(\mathbf{n}_{ab}\cdot\mathbf{p}_b)^2}{m_a^2 m_b^2}\right.\\
&\left. - 12\frac{(\mathbf{p}_a\cdot\mathbf{p}_b)(\mathbf{n}_{ab}\cdot\mathbf{p}_a)(\mathbf{n}_{ab}\cdot\mathbf{p}_b)}{m_a^2 m_b^2} - 3\frac{(\mathbf{n}_{ab}\cdot\mathbf{p}_a)^2(\mathbf{n}_{ab}\cdot\mathbf{p}_b)^2}{m_a^2 m_b^2}\right\} + \frac{1}{8}\sum_{a,b\neq a,c\neq a}\frac{m_a m_b m_c}{r_{ab}r_{ac}}\left\{18\frac{p_a^2}{m_a^2}\right.\\
&+ 14\frac{p_b^2}{m_b^2} - 2\frac{(\mathbf{n}_{ab}\cdot\mathbf{p}_b)^2}{m_b^2} - 50\frac{\mathbf{p}_a\cdot\mathbf{p}_b}{m_a m_b} + 17\frac{\mathbf{p}_b\cdot\mathbf{p}_c}{m_b m_c} - 14\frac{(\mathbf{n}_{ab}\cdot\mathbf{p}_a)(\mathbf{n}_{ab}\cdot\mathbf{p}_b)}{m_a m_b}\\
&\left. + 14\frac{(\mathbf{n}_{ab}\cdot\mathbf{p}_b)(\mathbf{n}_{ab}\cdot\mathbf{p}_c)}{m_b m_c} + \mathbf{n}_{ab}\cdot\mathbf{n}_{ac}\frac{(\mathbf{n}_{ab}\cdot\mathbf{p}_b)(\mathbf{n}_{ac}\cdot\mathbf{p}_c)}{m_b m_c}\right\}\\
&+ \frac{1}{8}\sum_{a,b\neq a,c\neq a}\frac{m_a m_b m_c}{r_{ab}^2}\left\{2\frac{(\mathbf{n}_{ab}\cdot\mathbf{p}_a)(\mathbf{n}_{ac}\cdot\mathbf{p}_c)}{m_a m_c} + 2\frac{(\mathbf{n}_{ab}\cdot\mathbf{p}_b)(\mathbf{n}_{ac}\cdot\mathbf{p}_c)}{m_a m_c} + 5\mathbf{n}_{ab}\cdot\mathbf{n}_{ac}\frac{p_c^2}{m_c^2}\right.\\
&\left. - \mathbf{n}_{ab}\cdot\mathbf{n}_{ac}\frac{(\mathbf{n}_{ac}\cdot\mathbf{p}_c)^2}{m_c^2} - 14\frac{(\mathbf{n}_{ab}\cdot\mathbf{p}_c)(\mathbf{n}_{ac}\cdot\mathbf{p}_c)}{m_c^2}\right\} + \frac{1}{4}\sum_{a,b\neq a}\frac{m_a^2 m_b}{r_{ab}^2}\left\{\frac{p_a^2}{m_a^2} + \frac{p_b^2}{m_b^2} - 2\frac{\mathbf{p}_a\cdot\mathbf{p}_b}{m_a m_b}\right\}\\
&+ \frac{1}{2}\sum_{a,b\neq a,c\neq a,b}\frac{m_a m_b m_c}{(r_{ab}+r_{bc}+r_{ca})^2}(n_{ab}^i + n_{ac}^i)(n_{ab}^j + n_{cb}^j)\left\{8\frac{p_{ai}p_{cj}}{m_a m_c} - 16\frac{p_{aj}p_{ci}}{m_a m_c}\right.\\
&\left. + 3\frac{p_{ai}p_{bj}}{m_a m_b} + 4\frac{p_{ci}p_{cj}}{m_c^2} + \frac{p_{ai}p_{aj}}{m_a^2}\right\} + \frac{1}{2}\sum_{a,b\neq a,c\neq a,b}\frac{m_a m_b m_c}{(r_{ab}+r_{bc}+r_{ca})r_{ab}}\\
&\left\{8\frac{\mathbf{p}_a\cdot\mathbf{p}_c - (\mathbf{n}_{ab}\cdot\mathbf{p}_a)(\mathbf{n}_{ab}\cdot\mathbf{p}_c)}{m_a m_c} - 3\frac{\mathbf{p}_a\cdot\mathbf{p}_b - (\mathbf{n}_{ab}\cdot\mathbf{p}_a)(\mathbf{n}_{ab}\cdot\mathbf{p}_b)}{m_a m_b} - 4\frac{p_c^2 - (\mathbf{n}_{ab}\cdot\mathbf{p}_c)^2}{m_c^2}\right.\\
&\left. - \frac{p_a^2 - (\mathbf{n}_{ab}\cdot\mathbf{p}_a)^2}{m_a^2}\right\} - \frac{1}{2}\sum_{a,b\neq a,c\neq b}\frac{m_a^2 m_b m_c}{r_{ab}^2 r_{bc}} - \frac{1}{4}\sum_{a,b\neq a,c\neq a}\frac{m_a m_b m_c^2}{r_{ab}r_{ac}^2} + \frac{1}{2}\sum_{a,b\neq a}\frac{m_a^3 m_b}{r_{ab}^3}\\
&- \frac{3}{4}\sum_{a,b\neq a,c\neq a}\frac{m_a^2 m_b m_c}{r_{ab}^2 r_{ac}} - \frac{3}{8}\sum_{a,b\neq a,c\neq a,b}\frac{m_a^2 m_b m_c}{r_{ab}r_{ac}r_{bc}} + \frac{3}{8}\sum_{a,b\neq a}\frac{m_a^2 m_b^2}{r_{ab}^3}\\
&- \frac{1}{64}\sum_{a,b\neq a,c\neq a,b}\frac{m_a^2 m_b m_c}{r_{ab}^3 r_{ac}^3 r_{bc}}\left\{18r_{ab}^2 r_{ac}^2 - 60r_{ab}^2 r_{bc}^2 - 24r_{ab}^2 r_{ac}(r_{ab}+r_{bc})\right.\\
&\left. + 60r_{ab}r_{ac}r_{bc}^2 + 56r_{ab}^3 r_{bc} - 72r_{ab}r_{bc}^3 + 35r_{bc}^4 + 6r_{ab}^4\right\} - \frac{1}{4}\sum_{a,b\neq a}\frac{m_a^2 m_b^2}{r_{ab}^3}. \qquad \text{(A.8)}
\end{aligned}
$$

And Finally the 2.5th Hamiltonian is

$$
H_{2.5PN} = \frac{1}{45}\dot{\chi}_{(4)ij}(\mathbf{x}_{a'},\mathbf{p}_{a'};t)\chi_{(4)ij}(\mathbf{x}_a,\mathbf{p}_a), \qquad \text{(A.9)}
$$

where

$$\chi_{(4)ij}(\mathbf{x}_a,\mathbf{p}_a) = \sum_a \frac{2}{m_a}\big((\mathbf{p}_a\cdot\mathbf{p}_a)\delta_{ij} - 3p_{ai}p_{aj}\big) + \sum_{a,b\neq a}\frac{m_a m_b}{r_{ab}}\big(3n_{abi}n_{abj}-\delta_{ij}\big), \tag{A.10}$$

and

$$\dot{\chi}_{(4)ij}(\mathbf{x}_{a'},\mathbf{p}_{a'}) = \sum_{a'}\frac{2}{m_{a'}}\Big[2\big(\dot{\mathbf{p}}_{a'}\cdot\mathbf{p}_{a'}\big)\delta_{ij} - 3(\dot{p}_{a'i}p_{a'j}+p_{a'i}\dot{p}_{a'j})\Big] + \sum_{a',b'\neq a'}\frac{m_{a'}m_{b'}}{r_{a'b'}^2}\Big[3(\dot{r}_{a'b'i}n_{a'b'j}+n_{a'b'i}\dot{r}_{a'b'j}) + (\mathbf{n}_{a'b'}\cdot\dot{\mathbf{r}}_{a'b'})(\delta_{ij}-9n_{a'b'i}n_{a'b'j})\Big]. \tag{A.11}$$

We approximate the derivatives $\dot{x}$ and $\dot{p}$ with the 1PN equations of motion:

$$(\dot{\mathbf{x}}_a)_1 = -\frac{p_a^2}{2m_a^3}\mathbf{p}_a - \frac{1}{2}\sum_{b\neq a}\frac{1}{r_{ab}}\left(6\frac{m_b}{m_a}\mathbf{p}_a - 7\mathbf{p}_b - (\mathbf{n}_{ab}\cdot\mathbf{p}_b)\mathbf{n}_{ab}\right), \tag{A.12}$$

$$(\dot{\mathbf{p}}_a)_1 = -\frac{1}{2}\sum_{b\neq a}\left[3\frac{m_b}{m_a}p_a^2 - 7(\mathbf{p}_a\cdot\mathbf{p}_b) - 3(\mathbf{n}_{ab}\cdot\mathbf{p}_a)(\mathbf{n}_{ab}\cdot\mathbf{p}_a)\right]\frac{\mathbf{n}_{ab}}{r_{ab}^2} + \sum_{b\neq a,c\neq a}\frac{m_a m_b m_c}{r_{ab}^2 r_{ac}}\mathbf{n}_{ab} + \sum_{b\neq a,c\neq b}\frac{m_a m_b m_c}{r_{ab}^2 r_{bc}}\mathbf{n}_{ab} - \frac{1}{2}\sum_{a\neq b}\left[\frac{(\mathbf{n}_{ab}\cdot\mathbf{p}_b)\mathbf{p}_a + (\mathbf{n}_{ab}\cdot\mathbf{p}_a)\mathbf{p}_b}{r_{ab}^2}\right]. \tag{A.13}$$

The primed variables in the equation for $\dot{\chi}$ are unaffected by the partial derivatives in the Hamiltonian equations, so the 2.5PN equations of motion are

$$(\dot{\mathbf{x}}_a)_{2.5} = \frac{1}{45}\dot{\chi}_{(4)ij}(\mathbf{x}_a,\mathbf{p}_a;(\dot{\mathbf{x}}_a)_1,(\dot{\mathbf{p}}_a)_1,t)\frac{\partial}{\partial\mathbf{p}_a}\chi_{(4)ij}(\mathbf{x}_a,\mathbf{p}_a), \tag{A.14}$$

$$(\dot{\mathbf{p}}_a)_{2.5} = -\frac{1}{45}\dot{\chi}_{(4)ij}(\mathbf{x}_a,\mathbf{p}_a;(\dot{\mathbf{x}}_a)_1,(\dot{\mathbf{p}}_a)_1,t)\frac{\partial}{\partial\mathbf{x}_a}\chi_{(4)ij}(\mathbf{x}_a,\mathbf{p}_a). \tag{A.15}$$

The equations of motion are calculated using Mathematica, which outputs the equations as optimized code for C and FORTRAN.

# Bibliography


[1] M. Volonteri, "Formation of supermassive black holes," The Astronomy and Astrophysics Review **18,** 279–315 (2010).

[2] M. Colpi, "Massive Binary Black Holes in Galactic Nuclei and Their Path to Coalescence," in *The Physics of Accretion onto Black Holes*, Vol. 49 of *Space Sciences Series of ISSI*, M. Falanga, T. Belloni, P. Casella, M. Gilfanov, P. Jonker, and A. King, eds., (Springer New York, 2015), pp. 189–221.

[3] G. Schafer, "Post-Newtonian Approximations and Equations of Motion in General Relativity," Astrophys. J. **1,** 44–53 (1997).

[4] E. R.-R. Johan Samsing, Morgan MacLeod, "The Formation of Eccentric Compact Binary Inspirals and the Role of Gravitational Wave Emission in Binary-Single Stellar Encounters," Astrophys. J. **1,** 1–22 (2013).

[5] J. Barrow-Green, F. Diacu, and P. Holmes, "Poincar e and the three body problem," ADDITIVE NUMBER THEORY: THE CLASSICAL BASES **31,** 121 (1999).

[6] J. H. Steffen *et al.*, "Transit timing observations from Kepler–VII. Confirmation of 27 planets in 13 multiplanet systems via transit timing variations and orbital stability," Monthly Notices of the Royal Astronomical Society **428,** 1077–1087 (2013).

[7] B. Gladman, "Dynamics of systems of two close planets," Icarus **106,** 247–263 (1993).

[8] E. Hairer, R. I. McLachlan, and A. Razakarivony, "Achieving BrouwerâĂŹs law with implicit Runge–Kutta methods," BIT Numerical Mathematics **48,** 231–243 (2008).

[9] M. Valtonen and H. Karttunen, *The three-body problem* (Cambridge University Press, 2006).

[10] A. Morbidelli, *Modern Celestial Mechanics* (CRC Press, 2002).

[11] S. L. W. M. Patricia T. Boyd, "Chaotic Scattering in the Gravitational Three-Body Problem," Am. J. Phys. Chaos. **3,** 507–523 (1993).

[12] G. Schäfer, "Post-Newtonian methods: Analytic results on the binary problem," in *Mass and Motion in General Relativity* (Springer, 2011), pp. 167–210.

[13] P. Jaranowski and G. Schäfer, "Radiative 3.5 post-Newtonian ADM Hamiltonian for many-body point-mass systems," Physical Review D **55,** 4712 (1997).

[14] J. Jay, "Chaotic Scattering in General Relativity," Brigham Young University Senior Thesis (Brigham Young University, 2015).

[15] M. Anderson, E. W. Hirschmann, L. Lehner, S. L. Liebling, P. M. Motl, D. Neilsen, C. Palenzuela, and J. E. Tohline, "Simulating binary neutron stars: Dynamics and gravitational waves," Physical Review D **77,** 024006 (2008).

[16] J. P. G. Vilchis, "Numerical Simulations of Three Black Holes," Ph.D. dissertation (the Friedrich-Schiller-University, Jena,Germany., 1979).

[17] N. A. R. Center, "Kepler Table of Confirmed Planets,", 2014.

[18] L. Petzold and A. Hindmarsh, "Lsoda," Computing and Mathematics Research Division, I-316 Lawrence Livermore National Laboratory, Livermore, CA 94550 (1997).

[19] N. S. W. G. Hairer, E., *Solving Ordinary Differential Equations I: Nonstiff Problems* (1987), Vol. 2.

# Index